Measuring Cortico-Cortical Connectivity Matrices with Diffusion Spectrum Imaging

David S. Tuch[1], Mette R Wiegell[1], Timothy G. Reese[1], John W. Belliveau[1], Van J. Wedeen[1]
[1]Massachusetts General Hospital, NMR Center, 149 13th Street, Charlestown, Massachusetts USA;

Introduction

The tractography problem is concerned with the inference of neural connectivity from magnetic resonance diffusion images [1-3]. Canonically, neural connectivity is described by a connectivity matrix, expressing the degree of connectivity between any two locations in the brain. Here, we describe a method to derive cortical connectivity matrices from diffusion images. The method entails three steps: (i) diffusion spectrum imaging (DSI) [4] to resolve intravoxel orientational heterogeneity up to the cortical margin, (ii) solution of optimal paths between all pairs of points in a set of defined cortical surface points, and (iii) tabulation of the fitness of the optimal paths to construct a connectivity matrix.

Given the interest of the present study in cortico-cortical connectivity we employed DSI to resolve the intravoxel fiber heterogeneity of the subcortical white matter. The DSI method, a relative of dynamic NMR microscopy [5], measures the microscopic spin displacement function *in toto*. The structure of the spin displacement function, which we refer to as the diffusion spectrum, can resolve complex intravoxel distributions of fiber orientation including white fiber intersections irresolvable by the tensor model. For example, at intersections of white matter fascicles the diffusion spectrum exhibits multiple discrete peaks with each peak directed towards a component fiber population. In addition to exhibiting complex, multi-modal structure in deep white matter intersections the diffusion spectrum exhibits complex, clearly non-mono-Gaussian structure at the subcortical margin [4].

To test the ability of DSI and the connectivity matrix algorithm to demonstrate relative connectivity within and between cortico-cortical networks, we mapped the connectivity matrix for a uniform series of points on the cortical surface spanning the visual and sensorimotor areas.

Methods

Image Acquisition Cardiac-gated, multi-slice, balanced-echo [6] diffusion images were acquired at 3T (Siemens, Allegra) on a normal volunteer with TE/Δ/δ=140/65/60ms, TR=4slices/2RR intervals, and 4×4×4mm voxel resolution. The balanced echo sequence consisted of 90-g-180-g-180-g-acq where the placement of the 180-pair was optimized to eliminate Eddy current distortions [6]. The diffusion gradient sampling scheme consisted of a keyhole Cartesian acquisition to include the set of points in q-space lying on a Cartesian grid ($\Delta q=0.01\mu^{-1}$) within a sphere of radius $q_{max}=0.1\mu^{-1}$, for a total of 500 sampling points [4] (Fig. 1). The above sampling scheme provided a diffusion spectrum resolution of $(2q_{max})^{-1}=4.5\mu$ and FOV $(2\Delta q)^{-1}=45\mu$. The displacement spectra P(r) were obtained by discrete Fourier transform of the modulus of the echo signal as a function of q for each voxel.

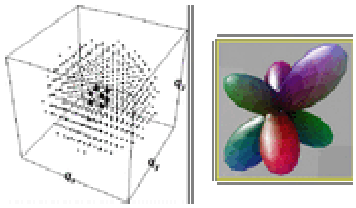


Fig 1. (a) Keyhole Cartesian DSI sampling scheme. The heavy dots depict a typical DTI acquisition. (b) Sample diffusion spectrum from three-way crossing of the corona radiata, corpus callosum, and superior longitudinal fasciculus.

Connectivity Algorithm

The connectivity algorithm consists of calculating optimal paths between all the pairs of points in a set of cortical surface points, and then tabulating the fitness of the optimal paths to construct a connectivity matrix. The set of cortical surface points is designated $X=\{\mathbf{x}_p\}$. The path between two endpoints $\mathbf{x}_i$ and $\mathbf{x}_j$ in X is represented by a set W_{ij} of n 'control points' and the 2 endpoints, $W_{ij}=\mathbf{x}_i,\mathbf{x}_1,...,\mathbf{x}_n,\mathbf{x}_j$. The energy of a path W_{ij} is defined as

$$E(W_{ij})=\sum_{Wij} P(\mathbf{x}_k, \alpha\mathbf{u}_k)+\gamma K$$

where $P(\mathbf{x}_k, \alpha\mathbf{u}_k)$ is the diffusion spectrum value at image location $\mathbf{x}_k$ and displacement $\alpha\mathbf{u}_k$, $\alpha(=25\mu)$ is a length-scale constant and $\mathbf{u}_k$ is the unit tangent vector to the fiber at location $\mathbf{u}_k$, γ is a stiffness weight, and K is the stiffness energy of the path. The optimal (least-energetic) path W^*_{ij} is found by solving for the control points which minimize the path energy defined in Eqn. 1. The optimal control points are solved for using a Monte Carlo simulated annealing algorithm [7]. The connectivity C_{ij} between the points $\mathbf{x}_i$ and $\mathbf{x}_j$ is then taken as the negative energy of the path, specifically,

$$C_{ij}=-E(W^*_{ij}).$$

For the connectivity matrix calculation performed here, 25 cortical surface points were placed along a saggital line 9mm from the midline running from the occipital pole to the middle of the superior frontal gyrus (Fig. 2a).

Results

The connectivity matrix (Fig. 2b) revealed increased connectivity within the occipital cortex and within the frontal sensorimotor cortex including between the motor and pre-motor areas. A relatively sharp connectivity boundary was observed between the visual and sensorimotor areas. Additionally, reduced connectivity was seen between the occipital and frontal areas.

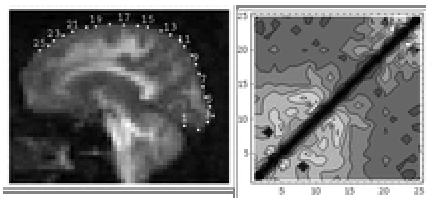


Fig 2. (a) Twenty-five cortical surface points, and (b) computed connectivity matrix. Lighter is higher connectivity.

Discussion

We have described a procedure for deriving a cortical connectivity matrix from diffusion images. Whereas differential tractography methods are limited to individual tract solutions the connectivity matrix framework can describe multiple anatomical projections and their relative significance. Lastly, the connectivity matrix lends itself naturally to network models of functional brain activity.

References

1. Conturo, T.E., et al. PNAS. 96:10422-7, 1999.
2. Mori, S., et al. Ann Neurol. 45:265-9, 1999.
3. Wedeen, V.J., et al. Proc HBM, p. 69, 1995.
4. Wedeen, V.J., et al. Eighth ISMRM, Denver., CO, p. 82, 2000.
5. Callaghan, P.T. Principles of nuclear magnetic resonance microscopy, Oxford, 1993.
6. Reese, T.G., et al. Sixth ISMRM, Sydney, Australia, p. 663, 1998.
7. Van Laarhoven, P.J.M., et al. Simulated annealing: theory and applications, Kluwer, 1987.